nature metabolism

ARTICLES

https://doi.org/10.1038/s42255-019-0045-8

Characterization of hypoxia-associated molecular features to aid hypoxia-targeted therapy

Youqiong Ye[1,15], Qingsong Hu[2,15], Hu Chen[3,4], Ke Liang[2], Yuan Yuan[3], Yu Xiang[1], Hang Ruan[1], Zhao Zhang[1], Anren Song[1], Huiwen Zhang[1], Lingxiang Liu[5], Lixia Diao[3], Yanyan Lou[6], Bingying Zhou[7], Li Wang[7], Shengtao Zhou[8], Jianjun Gao[9], Eric Jonasch[9], Steven H. Lin[10], Yang Xia[1,11], Chunru Lin[2,11], Liuqing Yang[2,11]*, Gordon B. Mills[12,13]*, Han Liang[3,4,11,12]* and Leng Han[1,11,14]*

Tumour hypoxia is a major contributor to resistance to anticancer therapies. Given that the results of hypoxia-targeted therapy trials have been disappointing, a more personalized approach may be needed. Here, we characterize multi-omic molecular features associated with tumour hypoxia and identify molecular alterations that correlate with both drug-resistant and drug-sensitive responses to anticancer drugs. Based on a well-established hypoxia gene expression signature, we classify about 10,000 tumour samples into hypoxia score-high and score-low groups across different cancer types from The Cancer Genome Atlas (TCGA) and demonstrate their prognostic associations. Then, we identify various types of molecular features associated with hypoxia status that correlate with drug resistance but, in some cases, also with drug sensitivity, contrasting the conventional view that hypoxia confers drug resistance. We further show that 110 out of 121 (90.9%) clinically actionable genes can be affected by hypoxia status and experimentally validate the predicted effects of hypoxia on the response to several drugs in cultured cells. Our study provides a comprehensive molecular-level understanding of tumour hypoxia and may have practical implications for clinical cancer therapy.

Hypoxia is a condition characterized by a limited oxygen supply; it is a feature of most tumours and has been correlated with advanced tumour progression, treatment resistance and poor clinical outcome[1,2]. Tumour hypoxia is linked to many cancer 'hallmarks', including impaired immune responses, metabolic reprogramming, increased cancer stem cells, stimulation of tumour vascularization, promotion of tumour invasion and metastasis, increased genomic instability, facilitation of apoptosis, and reduced cell proliferation[3]. Nevertheless, it is still difficult to define hypoxia status in tumours because of variations in oxygen levels among different tissues. Researchers have employed different methods to diagnose tumour hypoxia, including direct methods (for example, oxygen electrode and phosphorescence quenching), physiological methods (for example, photoacoustic tomography and near-infrared spectroscopy/tomography) and/or endogenous markers of hypoxia (for example, hypoxia-inducible factor 1-alpha (HIF-1α) and glucose transporter 1)[2], but none of these methods can be easily applied to large numbers of patient samples. Therefore, several recent studies have identified gene expression signatures that reflect hypoxia status[4–6]. Among them, a 15-gene signature appears to perform the best[5,7].

The tumour hypoxia microenvironment is associated with multiple layers of molecular alterations, from genomics and epigenomics to transcriptomics and proteomics. Hypoxia drives transient site-specific copy alterations[8] and increases the mutation frequency of key cancer genes[9]. Hypoxia induces the hypermethylation of promoter regions for several tumour suppressor genes, such as phosphatase and tensin homologue (*PTEN*) and APC regulator of WNT signalling pathway (*APC*), and thus leads to low expression of these tumour suppressors[7]. Furthermore, hypoxia dysregulates genes in cancer-related pathways, such as the glycolytic pathway and phosphoinositide 3-kinase (PI3K)/protein kinase B (PKB/Akt)/mammalian target of rapamycin (mTOR) pathway[10], as well as pro-angiogenic factors[11] and oncogenic growth factors[12]. In addition, in response to hypoxia, micro RNAs (miRNAs) linked to multiple key signalling pathways, such as miR-210, are altered[13]. Hypoxia also profoundly impacts protein synthesis and phosphorylation, such as the activation of PKR-like endoplasmic reticulum kinase (PERK) and phosphorylation of eukaryotic initiation factor 2-alpha (eIF2α)[14]. Taken together, previous studies have established that hypoxia can lead to

[1]Department of Biochemistry and Molecular Biology, The University of Texas Health Science Center at Houston-McGovern Medical School, Houston, TX, USA. [2]Department of Molecular and Cellular Oncology, The University of Texas MD Anderson Cancer Center, Houston, TX, USA. [3]Department of Bioinformatics and Computational Biology, The University of Texas MD Anderson Cancer Center, Houston, TX, USA. [4]Graduate Program in Quantitative and Computational Biosciences, Baylor College of Medicine, Houston, TX, USA. [5]Department of Oncology, The First Affiliated Hospital of Nanjing Medical University, Nanjing, China. [6]Division of Hematology and Oncology, Mayo Clinic, Jacksonville, FL, USA. [7]State Key Laboratory of Cardiovascular Disease, Fuwai Hospital, National Center for Cardiovascular Diseases, Chinese Academy of Medical Sciences and Peking Union Medical College, Beijing, China. [8]Department of Obstetrics and Gynecology, Key Laboratory of Birth Defects and Related Diseases of Women and Children of MOE and State Key Laboratory of Biotherapy, West China Second University Hospital, Sichuan University and Collaborative Innovation Center, Chengdu, China. [9]Department of Genitourinary Medical Oncology, The University of Texas MD Anderson Cancer Center, Houston, TX, USA. [10]Department of Radiation Oncology, Division of Radiation Oncology, The University of Texas MD Anderson Cancer Center, Houston, TX, USA. [11]MD Anderson Cancer Center UTHealth Graduate School of Biomedical Sciences, Houston, TX, USA. [12]Department of Systems Biology, The University of Texas MD Anderson Cancer Center, Houston, TX, USA. [13]Knight Cancer Institute, Oregon Health and Science University, Portland, OR, USA. [14]Center for Precision Health, The University of Texas Health Science Center at Houston, Houston, TX, USA. [15]These authors contributed equally: Youqiong Ye, Qingsong Hu. *e-mail: lyang7@mdanderson.org; millsg@ohsu.edu; hliang1@mdanderson.org; leng.han@uth.tmc.edu

multiple layers of molecular changes and thus plays a pivotal role in cancer development.

Hypoxia is a major contributor to resistance to anticancer therapies, including chemotherapy, radiation therapy, targeted therapy and immunotherapy, thereby making hypoxia-targeted therapies attractive[15]. Severe hypoxia can induce resistance to chemotherapy in cervical tumours[16], and blocking HIF activity in breast cancer can increase the effect of chemotherapy treatment[17]. Hypoxic tumours have not responded well to radiation therapy in head and neck cancer[18]. Hypoxia can also cause resistance to gefitinib in both epidermal growth factor receptor (EGFR) mutant and wild-type non-small-cell lung cancer (NSCLC)[19]. Metformin-induced reduction of tumour hypoxia can potentiate the efficacy of immunotherapy with the PD-1 checkpoint inhibitor[20]. Thus, combining hypoxia-targeted therapy with other anticancer therapies would improve treatment efficacy. Indeed, combining the HIF-1α inhibitor with a molecular-targeted agent (for example, T40214, a phosphorylated signal transducer and activator of transcription 3 inhibitor)[21] or with a chemotherapeutic agent (for example, cisplatin)[22] has demonstrated greater clinical efficacy than either therapy alone. Strikingly, changes in hypoxic cells can also result in sensitivity to specific therapies[15]. For example, some tumours appear to be more sensitive to the poly(ADP-ribose) polymerase (PARP) inhibitors, veliparib and olaparib, under hypoxic conditions[23,24]. Patients with kidney cancers who had high levels of HIF-1α or HIF-2α responded better to sunitinib[25]. These studies suggest that the contribution of hypoxia status in cancer treatment is complex. Unfortunately, the results of hypoxia-targeted therapy trials, which have included evofosfamide and tarloxotinib bromide in lung cancer[26], 1-methylpropyl 2-imidazolyl disulfide in pancreatic cancer[27] and tirapazamine and nitroglycerin in lung cancer[28,29], have been disappointing. There is still a lack of predictive therapeutic biomarkers to make hypoxia-targeted therapy part of standard treatments[26]. The availability of genomic, epigenomic, transcriptomic and proteomic profiles across a broad range of cancer types from the TCGA project[30,31] provides an unprecedented opportunity to explore hypoxia-associated molecular signatures in great depth.

Results

Rigorous classification of hypoxia status by an established gene expression signature. To classify the hypoxia status of tumour samples, we focused on a 15-gene expression signature[6,7,32] that was shown to be the best performer in a recent comprehensive study assessing the robustness of different hypoxia signatures[5]. We performed multiple analyses to validate its performance and assess the robustness of this hypoxia signature. First, we collected ten independent gene expression datasets of cancer cell lines and tumour fragments of multiple cancer types under hypoxic and normoxic conditions (Supplementary Table 1). We calculated a hypoxia score for each sample based on this 15-gene signature. Indeed, in all cases, cells under the hypoxic conditions showed significantly higher hypoxia scores than those under the normoxic conditions (Fig. 1a–k). Second, the score for this signature highly correlated with the hypoxia scores based on the other two hypoxia signatures (the Winter[33] and Hu[34] signatures; Fig. 1l). The observed consistency suggests that the 15-gene signature is robust and that different classifiers would lead to similar groups. These results demonstrate the robustness of the 15-gene signature to define hypoxia status in different cancer types.

To classify the hypoxia status of tumour samples, we analysed 24 TCGA cancer types with a sample size ≥ 100 (ref. [30]). We further excluded kidney renal clear cell carcinoma (KIRC) and colon adenocarcinoma (COAD) samples with relatively high mutation frequency in von Hippel–Lindau tumour suppressor (*VHL*; ≥5%), which directly regulates HIF-1α to induce pseudohypoxia[35]. In each cancer type, we classified samples into hypoxia score-high, hypoxia score-low and hypoxia score-intermediate groups based on the unsupervised clustering pattern of the 15 genes (Fig. 2a and Supplementary Fig. 1; see Methods). In the 21 cancer types surveyed, both hypoxia score-high and hypoxia score-low groups contained ≥ 30 samples; we focused on these cancer types for the subsequent analysis. Indeed, the two sample groups showed distinct hypoxia score distributions (Supplementary Fig. 2a). To validate our messenger RNA (mRNA)-based sample classification, we further performed the analysis using independent proteomic data over the same TCGA sample sets. Using mass spectrum data from the Clinical Proteomic Tumor Analysis Consortium[36,37], we assessed the same hypoxia signature at the protein level and found that the signature was indeed enriched in the hypoxia score-high groups for both breast cancer (BRCA; normalized enrichment score (NES) = 1.92, false discovery rate (FDR) < 0.001) and ovarian serous cystadenocarcinoma (OV; NES = 2.15, FDR < 0.001; see Supplementary Fig. 2b). This is probably due to high correlations between mRNA and protein expression levels. Taken together, our analyses based on mRNA and protein expression data support the validation of our classification of hypoxia status across different cancer types.

The proportions of different hypoxia groups greatly varied among different cancer types (Fig. 2a). For example, in kidney renal papillary cell carcinoma (KIRP), 10.3% (30 out of 290) are hypoxia score-high samples versus 50.7% (147 out of 290) hypoxia score-low samples, while in thymoma (THYM), 48.3% (58 out of 120) are hypoxia score-high samples versus 27.5% (33 out of 120) hypoxia score-low samples (Fig. 2a and Supplementary Table 2). These results suggest that patients with different cancer types may have distinct response rates to hypoxia-targeted therapy. For example, for certain cancer types such as THYM, head and neck squamous cell carcinoma (HNSC), and lung squamous cell carcinoma (LUSC), larger proportions of patients are more likely to benefit from hypoxia-targeted therapy. In contrast, only a small proportion of patients with KIRP and prostate adenocarcinoma (PRAD) may benefit from hypoxia-targeted therapy since most of those tumours are classified as hypoxia score-low.

To assess the relevance of our sample classification in a clinical context, we examined the correlations of our hypoxia status classification with the overall survival time of patients. We observed that hypoxia score-high tumours were consistently associated with worse prognosis across cancer types in univariate or multivariate survival analysis using the Cox proportional hazards model (Fig. 2b), such as HNSC (log-rank test, $P = 2.9 \times 10^{-4}$), and lung adenocarcinoma (LUAD; log-rank test, $P = 5.1 \times 10^{-4}$; Fig. 2c). These results suggest the potential prognostic power of our hypoxia status classification.

Global patterns of multidimensional hypoxia-associated molecular signatures across cancer types. To identify the molecular signatures associated with hypoxia status in cancer, we employed a propensity score algorithm[38] to reduce any potential confounding effects (Supplementary Fig. 3 and Supplementary Table 3), for example, sex, age at diagnosis, tumour purity, race and tumour stage[39,40] (see Methods). As outlined in Fig. 3a, we compared molecular features between the hypoxia score-high and score-low groups with balanced confounding factors. Molecular features of consideration included: mRNA expression (approximately 20,000 genes); protein expression (approximately 200 proteins); miRNA expression (approximately 2,000 miRNAs); DNA methylation (approximately 16,000 protein-coding genes); highly mutated genes (genes with > 5% mutation frequency in each cancer type); and significant somatic copy number alterations (SCNAs) identified by GISTIC2.0 (ref. [41]). We identified significantly differential features of these six types between the two hypoxia status groups (Fig. 3b and Supplementary Data 1; FDR < 0.05; see Methods).

The effects of hypoxia status on the molecular data for different cancer types varied significantly. For example, alterations of mRNA

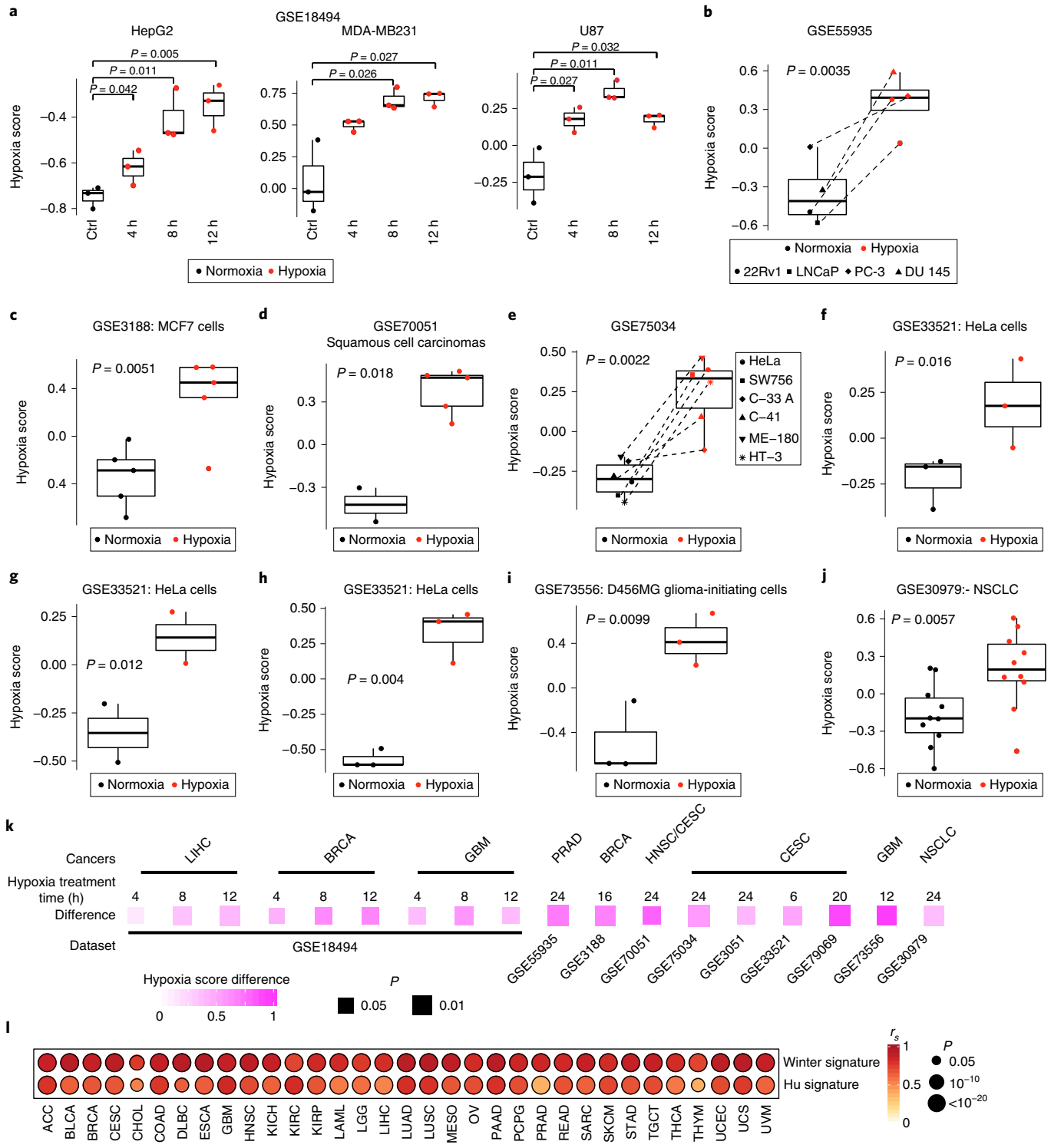

Fig. 1 | Validation of a 15-gene expression signature for hypoxia status. a–j, Hypoxia scores of cancer cell lines and tumour fragments under hypoxic and normoxic conditions in ten datasets. The boxes show the median ± 1 quartile, with the whiskers extending from the hinge to the smallest or largest value within 1.5× the interquartile range (IQR) from the box boundaries. A one-sided Student's *t*-test was used to assess the difference. *$P < 0.05$. Sample size for hypoxic conditions (**a**, $n = 3$; **b**, $n = 4$; **c**, $n = 5$; **d**, $n = 5$; **e**, $n = 6$; **f**, $n = 3$; **g**, $n = 2$; **h**, $n = 3$; **i**, $n = 3$; **j**, $n = 10$). Sample size for normoxic conditions (**a**, $n = 3$; **b**, $n = 4$; **c**, $n = 5$; **d**, $n = 2$; **e**, $n = 6$; **f**, $n = 3$; **g**, $n = 2$; **h**, $n = 3$; **i**, $n = 3$; **j**, $n = 10$). **k**, Summarized differences of hypoxia scores under hypoxic and normoxic conditions across the cancer cell line datasets from **a**–**j**. **l**, Spearman's correlation of hypoxia scores between this 15-gene signature and the other two gene signatures across cancer types ($n = 9{,}686$). The colour intensity indicates Spearman's rank correlation coefficient (r_s); the point size indicates *P* for the Spearman's rank correlation. ACC, adenoid cystic carcinoma; CHOL, cholangiocarcinoma; DLBC, diffuse large B-cell lymphoma; KICH, kidney chromophobe; LAML, acute myeloid leukaemia; MESO, mesothelioma; PCPG; pheochromocytoma and paraganglioma; READ, rectum adenocarcinoma; THCA, thyroid carcinoma; UCEC, uterine corpus endometrial carcinoma; UCS, uterine carcinosarcoma; UVM, uveal melanoma.

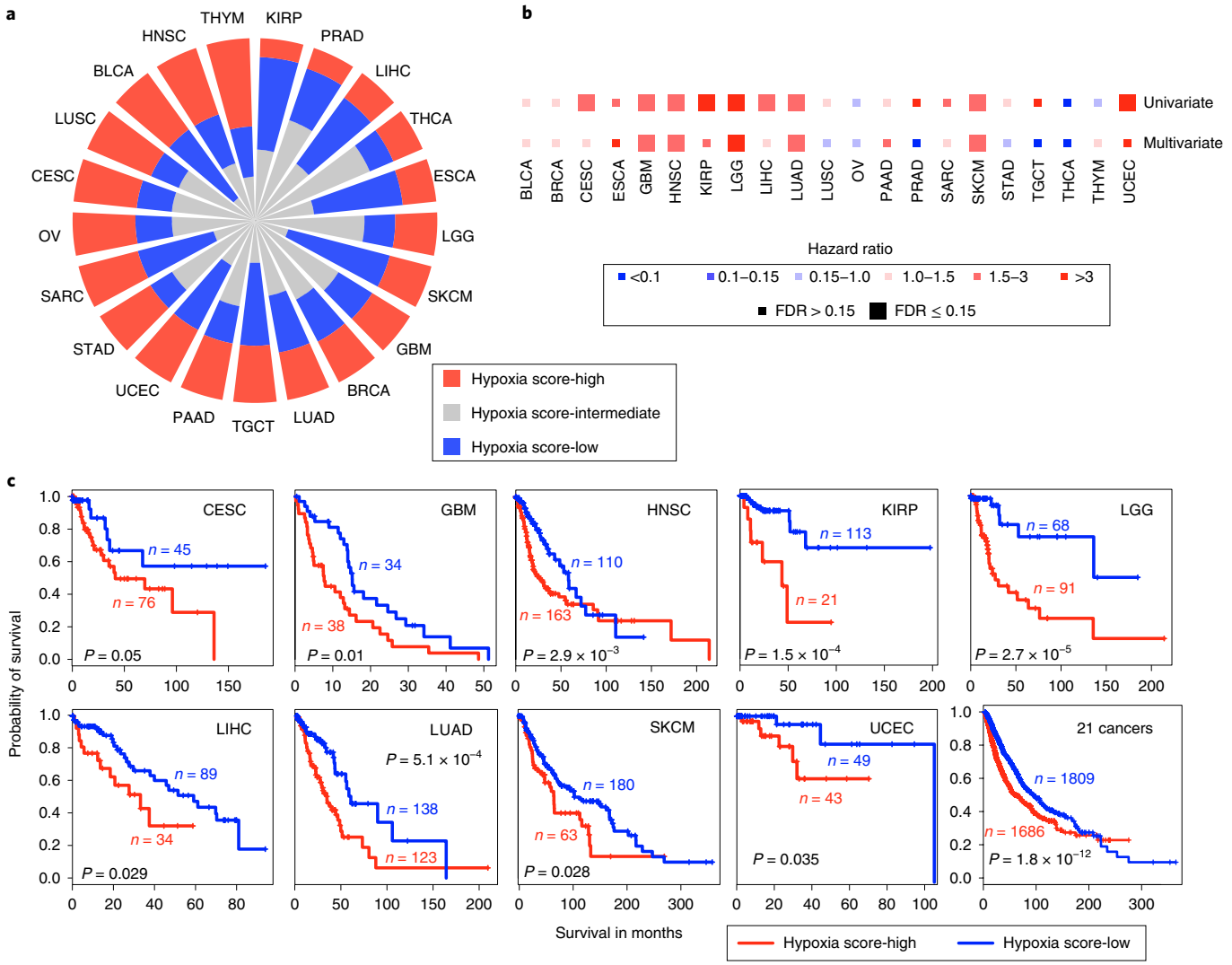

Fig. 2 | Classification of hypoxia status across different cancer types. a, Percentage of samples with hypoxia score-high, score-low and score-intermediate classifications across multiple cancer types based on this 15-gene signature. **b**, Association of hypoxia status with patient overall survival times based on both univariate and multivariate Cox proportional hazards models in different cancer types ($n = 3,495$). Size denotes statistical significance at a given FDR; colour denotes the hazard ratio. **c**, Kaplan–Meier curves show that hypoxia score-high status is associated with worse survival time in multiple cancer types. A two-sided log-rank test $P < 0.05$ is considered as a statistically significant difference.

expression ranged from 399 genes in OV to 4,795 genes in testicular germ cell tumours (TGCTs; Fig. 3b). Alterations of miRNA expression ranged from 2 in skin cutaneous melanoma (SKCM) to 213 in THYM. Stomach adenocarcinoma (STAD) showed the largest number of alterations at the protein level, while THYM showed the largest number of alterations in DNA methylation and BRCA showed the largest number of SCNAs. The total number of hypoxia-associated features across multiple layers also varied. For example, STAD had many hypoxia-associated features in six molecular layers, including 4,169 mRNAs, 186 miRNAs, 91 proteins, 294 methylation probes, 1 gene mutation and 10 SCNAs, while glioblastoma multiforme (GBM) had hypoxia-associated features in 629 mRNAs and 5 proteins. Furthermore, previous studies demonstrated the effects of hypoxia status on metabolomics[42]. Based on 399 metabolites from 23 TCGA BRCA samples[43], we observed that 86 metabolites positively correlated with hypoxia score ($r_s > 0.3$, $P < 0.05$; Supplementary Fig. 4a). We further identified 45 metabolites that were upregulated in 7 hypoxia score-high samples compared to 6 hypoxia score-low samples (two-sided Student's *t*-test, $P < 0.05$; Supplementary Fig. 4b). These results provide an overview of the molecular differences associated with hypoxia status across tumour lineages.

To assess the potential effects of hypoxia-associated features on drug response, we focused on 1,060 genes with at least 1 type of hypoxia-associated molecular signature in at least 9 cancer types. We calculated Spearman's rank correlations between the expression of these genes and drug sensitivity for 252 anticancer drugs from the Genomics of Drug Sensitivity in Cancer (GDSC)[44] across 1,074 cancer cell lines. These anticancer drugs target multiple biological processes, including the chromatin signature, cell cycle, metabolism, EGFR signalling and receptor tyrosine kinase (RTK) signalling pathways. We identified 143 hypoxia-associated genes that significantly correlated with the sensitivity of at least three anticancer drugs ($|r_s| > 0.3$, FDR < 0.05; Fig. 3c, Supplementary Fig. 5 and Supplementary Data 2). For example, the protein level of transcriptional coactivator YAP1 is upregulated in hypoxia score-high samples in nine cancer types; its mRNA expression is linked to drug resistance to 49 anticancer drugs (for example, navitoclax, $r_s = 0.52$, FDR < 1.0×10^{-55}) and linked to drug sensitivity to five anticancer drugs in (for example, docetaxel, $r_s = -0.42$, FDR = 1.7×10^{-35}). Dysregulation of the RTK signalling pathway is an established feature in multiple cancer types and RTK signalling can be stimulated

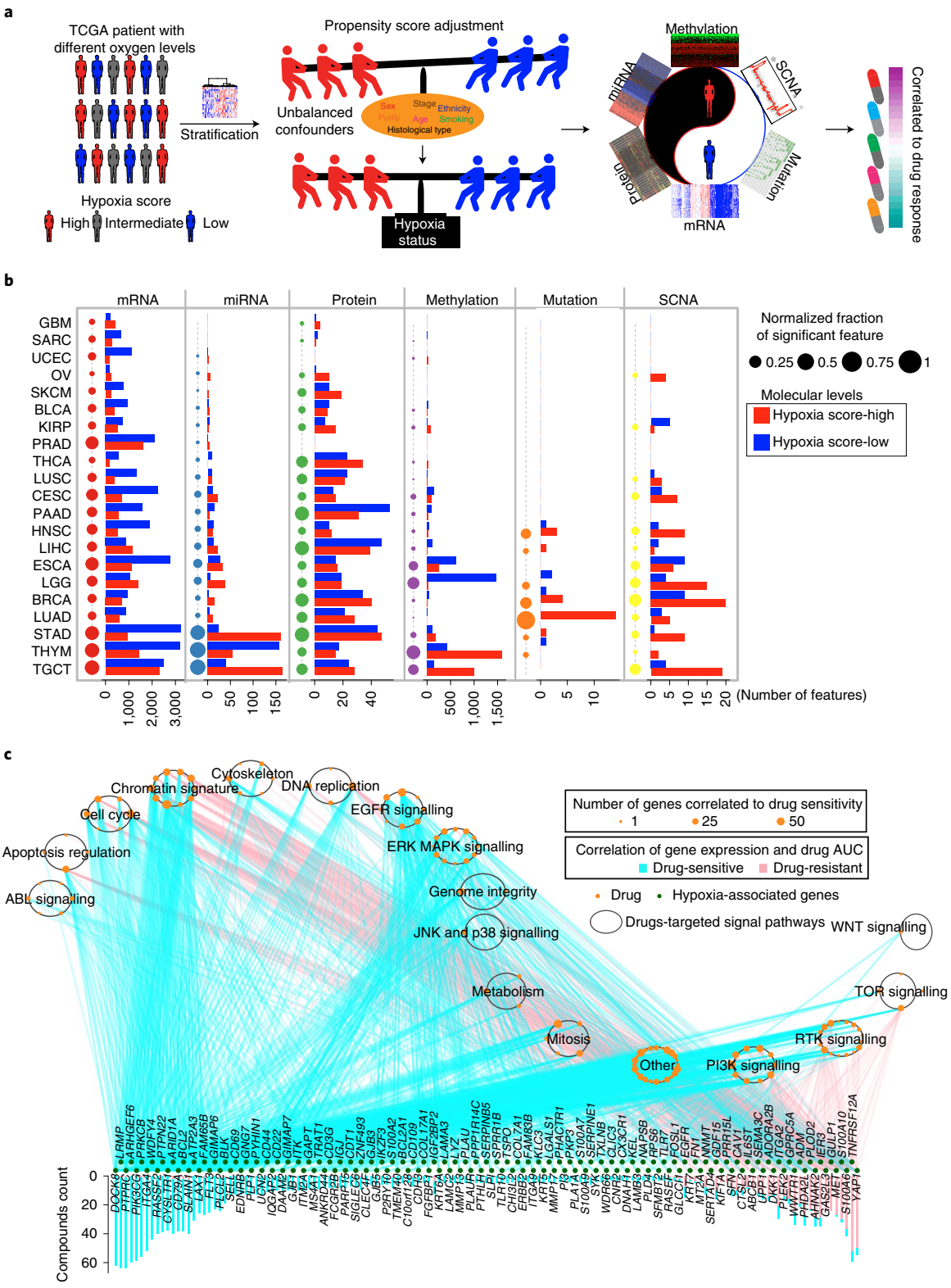

Fig. 3 | Overview of the propensity score algorithm and the hypoxia-associated molecular patterns across cancer types. a, Overview of the propensity score algorithm used to balance clinical features. **b**, Relative abundance and numbers of multidimensional hypoxia-associated molecular signatures identified by the propensity score algorithm. The percentage of significant features over the total features for each molecular signature in each cancer type is displayed as a solid circle; the number of significant features for the corresponding molecular signature is displayed as a bar plot. **c**, Association between mRNA expression levels of hypoxia-associated genes and drug sensitivity across 1,074 cancer cell lines by Spearman's rank correlation. The dark green dots along the *x* axis indicate hypoxia-related genes; the orange dots denote drugs that are clustered by different signalling pathways. The size of the orange dot indicates the number of genes correlated with drug sensitivity ($|r_s| > 0.3$, FDR < 0.05); the bar plot shows the number of drugs correlated with the genes. The pink and cyan lines indicate positive and negative correlation, respectively. JNK, Jun N-terminal kinase.

by hypoxia[45]. In our analysis, 19 drugs that targeted the genes involved in the RTK signalling pathway highly correlated with hypoxia-associated genes (Supplementary Fig. 5a). Taken together, our results across cancer cell lines show extensive interactions between hypoxia-associated molecular features and drug response, highlighting the potential of combining anti-hypoxia drugs with other cancer therapies.

Hypoxia effects on mRNA, miRNA, protein expression and DNA methylation. We observed significant alterations of mRNA expression across different cancer types. For example, several genes involved in invasion and metastasis were significantly biased in hypoxia score-high samples in TGCT, including neural cell adhesion molecule L1 (*L1CAM*; fold change = 4.5, FDR = 8.4×10^{-28}), lysyl oxidase homologue 4 (*LOX4*; fold change = 2.2, FDR = 1.6×10^{-5}), lysyl oxidase (*LOX*, fold change = 2.3, FDR = 1.5×10^{-7}) and tyrosine-protein kinase *MET* (fold change = 2.6, FDR = 1.6×10^{-9}). Genes involved in glycolysis, the p53 pathway, apoptosis, epithelial mesenchymal transition and angiogenesis were more likely to be upregulated in hypoxia score-high samples across cancer types (Supplementary Fig. 6a). These hypoxia-associated mRNA expression patterns are partially due to alterations of DNA methylation (Supplementary Fig. 6b). Indeed, the hypoxia-biased mRNA expression level of a gene tended to be the opposite of its DNA methylation level (Supplementary Fig. 6c), which is consistent with the view that hypermethylation generally leads to gene silencing, while hypomethylation results in gene overexpression[46].

To further investigate the effects of hypoxia on miRNA expression, we identified miRNAs that were differentially expressed between hypoxia score-high and hypoxia score-low samples. The hypoxia-induced miRNA, miR-210-3p[13], was upregulated in hypoxia score-high tumours in 16 cancer types (Fig. 4a and Supplementary Fig. 6d). In contrast, hypoxia-inhibited miR-139-3p[47] was downregulated in hypoxia score-high samples in four cancer types. Several target genes of miR-139-3p were upregulated, including: angiopoietin 1 (*ANGPT1*), which is associated with the promotion of vascularization; cathepsin C (*CTSC*), MET proto-oncogene, receptor tyrosine kinase (*MET*) and plasminogen activator, urokinase receptor (*PLAUR*), which are associated with invasion and metastasis; pyruvate kinase M1/2 (*PKM2*), which is related to metabolic reprogramming; and SRY-box 2 (*SOX2*) and WW domain containing transcription regulator 1 (*WWTR1*), which maintain cancer cell stemness. We further examined the targeted genes of 87 miRNAs that were also altered in at least three cancer types. We identified 3,793 miRNA-targeted genes with significantly opposing alterations. Genes targeted by these miRNAs are significantly enriched in cancer-related pathways, including the PI3K/Akt, Hippo, Ras, p53, EGFR, and HIF-1 signalling pathways (Fig. 4a). For example, miR-455-3p, miR-205-5p and 11 other miRNAs were significantly upregulated. Their target tumour suppressor gene, tumour protein p53 inducible nuclear protein 1 (*TP53INP1*), was significantly downregulated in hypoxia score-high samples in oesophageal carcinoma (ESCA), pancreatic adenocarcinoma (PAAD), STAD and TGCT. In contrast, miRNA-30a-5p/miRNA-30a-3p was significantly downregulated, and the target gene *MET*, a marker for invasion and metastasis and the therapeutic target of crizotinib in lung cancer[48], was upregulated in hypoxia score-high samples in GBM, low-grade glioma (LGG) and TGCT. Furthermore, hypoxia-associated miRNAs were highly associated with drug response in patients represented in the TCGA data (Supplementary Fig. 6d, upper panel). For example, the expression of hypoxia score-high-biased miR-210-3p highly correlated with the response to at least 1 drug in 13 cancer types (Supplementary Fig. 6e). In liver hepatocellular carcinoma (LIHC), this miR-210-3p negatively correlated (drug-sensitive) with the response to the serine-protein kinase ATM inhibitor KU-55933 ($r_s = -0.44$, FDR = 4.2×10^{-5}; Supplementary Fig. 6f), an inhibitor of ATM in the genome integrity pathway, while the expression of miR-210-3p positively correlated (drug-resistant) with vinorelbine ($r_s = 0.48$, FDR = 1.9×10^{-6}; Supplementary Fig. 6f), a microtubule destabilizer.

Using functional proteomic data of reverse-phase protein arrays that cover key cancer-related total and phosphorylated proteins, we identified hypoxia-associated protein alterations in cancer signalling pathways (Fig. 4b). For example, fibronectin, which positively regulates epithelial mesenchymal transition[49], was significantly upregulated in hypoxia score-high samples in seven cancer types. PTEN, which negatively regulates the PI3K/Akt signalling pathway[50], was significantly downregulated in hypoxia score-high samples in five cancer types. We observed that the anti-apoptosis protein, apoptosis regulator BCL2, was significantly downregulated in hypoxia score-high samples in seven cancer types, while the pro-apoptosis protein, caspase-7, was significantly upregulated in four cancer types. Furthermore, hypoxia-associated proteins correlated with the response to anticancer drugs (Fig. 4b). PTEN negatively correlated (drug-sensitive) with the response to dasatinib (LGG, $r_s = -0.47$, FDR = 5.8×10^{-5}), which targets SRC and many other kinases, but positively correlated (drug-resistant) with pictilisib (LGG, $r_s = 0.42$, FDR = 1.6×10^{-3}), a PI3K inhibitor (Supplementary Fig. 6g).

Integrative analysis of hypoxia-associated molecular features on drug response. To further understand the effects of the hypoxia microenvironment on drug response, we performed an integrative analysis to assess the associations between multidimensional hypoxia-associated molecular features and the response to anticancer drugs in TCGA patients (see Methods). Taking ESCA as an example, we identified 61 genes that were overexpressed in hypoxia score-high samples. These genes are hypomethylated and regulated by nine miRNAs. The expression levels of these genes negatively correlated (drug-sensitive) with the response to anticancer drugs, while their DNA methylation level and targeting miRNAs positively correlated (drug-resistant) with the same anticancer drugs. These drugs target important pathways, including the PI3K and ERK/mitogen-activated protein kinase (MAPK) signalling pathways (Fig. 5a). For example, EGFR was upregulated in hypoxia score-high tumours (fold change = 2.65, FDR = 3.2×10^{-5}; Fig. 5b) in ESCA, and EGFR expression negatively correlated (drug-sensitive) with the response to the RTK signalling pathway inhibitor crizotinib ($r_s = -0.28$, FDR = 0.02), the farnesyltransferase alpha subunit inhibitor FTI-277 ($r_s = -0.29$, FDR = 0.025), the Akt inhibitor A-443654 ($r_s = -0.26$, FDR = 0.015), serine/threonine-protein kinase B-raf (BRAF) inhibitor PLX4720 ($r_s = -0.31$, FDR = 2.0×10^{-3}) and the microtubule destabilizers vinorelbine ($r_s = -0.30$, FDR = 7.2×10^{-3}) and vinblastine ($r_s = -0.32$, FDR = 1.4×10^{-3}). EGFR showed hypomethylation in the promoter region (difference = −0.24, FDR = 4.5×10^{-8}); the methylation level of EGFR positively correlated (drug-resistant) with the response to A-443654 ($r_s = 0.34$, FDR = 5.5×10^{-4}), PLX4720 ($r_s = 0.47$, FDR = 5.3×10^{-7}), vinblastine ($r_s = 0.38$, FDR = 5.2×10^{-5}) and vinorelbine ($r_s = 0.32$, FDR = 2.3×10^{-3}). Meanwhile, four miRNAs that target EGFR showed significant downregulation in hypoxia score-high tumours (miR-375: fold change = −13.5, FDR = 4.4×10^{-9}; miR-153-5p: fold change = −2.03, FDR = 5.2×10^{-4}; miR-200a-3p: fold change = −2.4, FDR = 4.6×10^{-3}; miR-146a-5p: fold change = −2.5, FDR = 9.8×10^{-7}). These miRNAs positively correlated (drug-resistant) with the corresponding drugs that have negative correlations with EGFR expression. For example, miR-375 positively correlated (drug-resistant) with A-443654 ($r_s = 0.37$, FDR = 9.0×10^{-4}), PLX4720 ($r_s = 0.39$, FDR = 9.4×10^{-5}) and vinblastine ($r_s = 0.35$, FDR = 8.5×10^{-4}); miR-200a-3p positively correlated (drug-resistant) with A-443654 ($r_s = 0.35$, FDR = 1.3×10^{-4}), PLX4720 ($r_s = 0.29$, FDR = 6.1×10^{-3}) and vinblastine ($r_s = 0.44$, FDR = 1.2×10^{-5}). For 29 genes overexpressed in hypoxia score-low samples, we also observed a similar regulatory network in that the

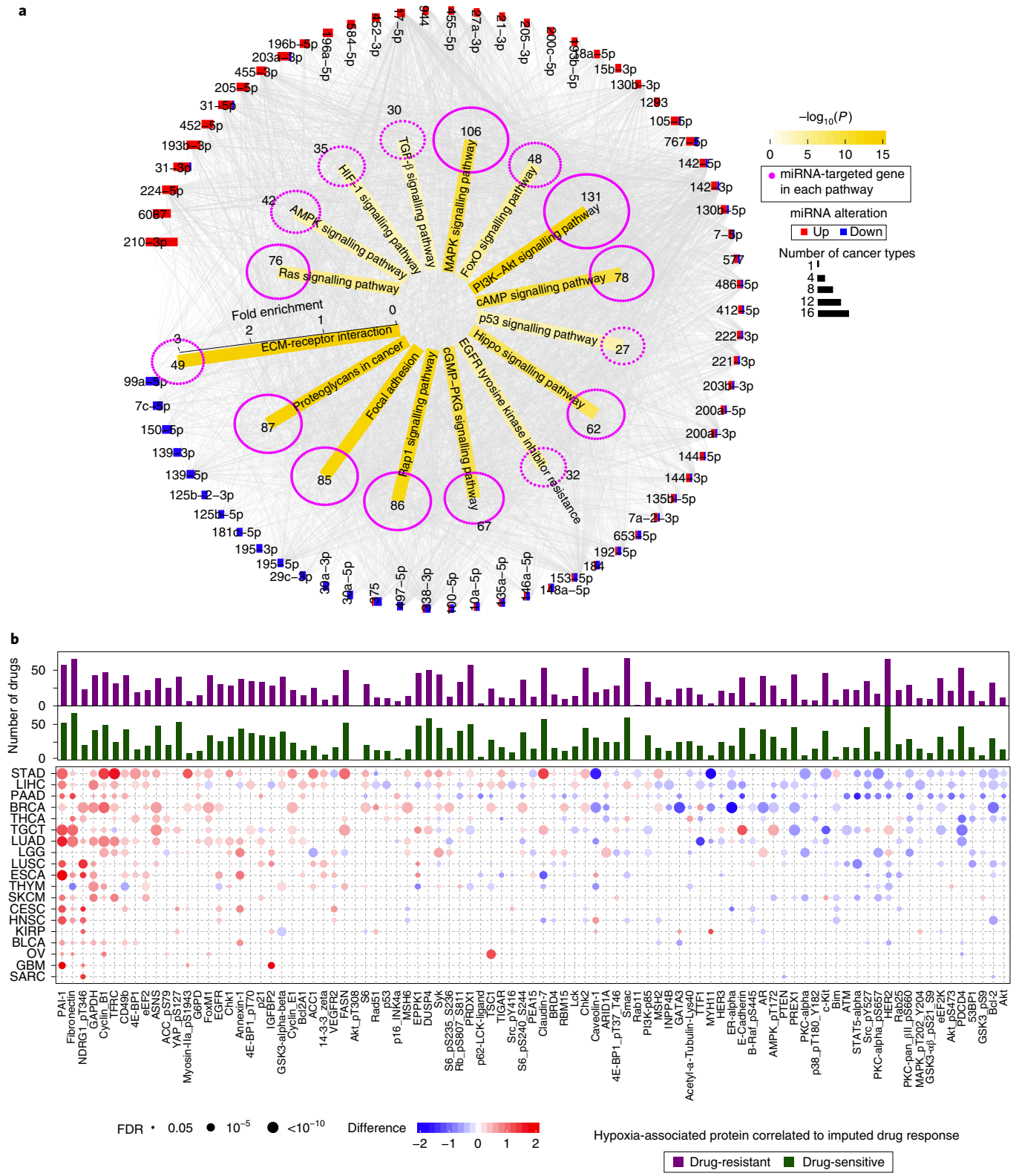

Fig. 4 | Hypoxia-associated miRNA and protein signatures. a, Hypoxia-associated, miRNA-regulated mRNA expression in multiple key signalling pathways. Number of cancer types with miRNA alterations in hypoxia score-high tumours (outer loop). 'miR' is omitted from the name of the miRNA. Genes are marked as magenta dots and organized in pathways (middle loop). The gold bar denotes enrichment of miRNA-targeted genes in the signalling pathways (inner loop); Fisher's exact test, with $P < 0.05$ as statistically significant. The grey lines link the miRNAs and their targeted genes. **b**, Alterations of protein or protein phosphorylation in hypoxia score-high samples in at least three cancer types. The upper panel bars display the accumulated number of drugs positively (dark magenta) or negatively (dark green) correlated with hypoxia-associated proteins in different cancer types. The correlation was performed by Spearman's rank correlation. Statistical analysis was performed using a propensity score algorithm to identify hypoxia-associated miRNAs and proteins; details are given in the Methods. AMPK, 5′-AMP-activated protein kinase; FoxO, forkhead box, class O; Rap1, Ras-related protein 1; TGF-β, transforming growth factor-beta.

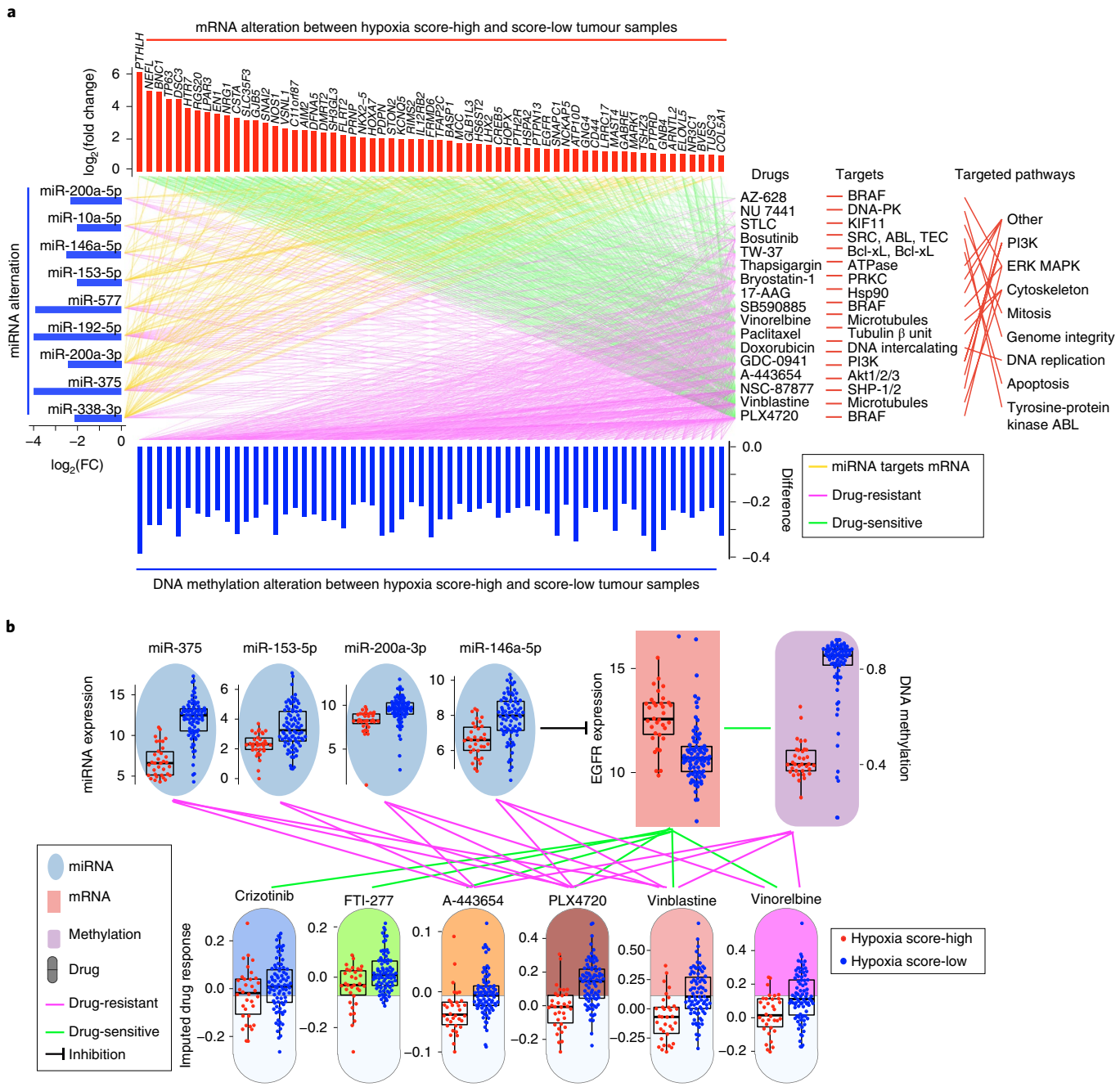

Fig. 5 | Effects of multidimensional hypoxia-associated signatures on drug response. a, Interaction of hypoxia-associated mRNAs, DNA methylation, miRNAs and drug response. Upregulated genes (red bars in upper panel) in hypoxia score-high ESCA negatively correlate (green lines, drug-sensitive) with the response to 17 drugs. Downregulated miRNAs (blue bars, left panel), hypomethylation (blue bars, bottom panel) for the corresponding upregulated genes positively correlate (magenta lines, drug-resistant) to drug response. The target genes and targeted pathways of drugs are listed in the panel to the right. The gold line indicates miRNA-targeted mRNAs; the red line links the drug to its target and targeted pathway. DNA-PK, DNA-dependent protein kinase; Hsp90, heat shock protein 90; KIF11, kinesin family member 11; PRKC, serine/threonine-protein kinase; SHP-1/2, Src homology 2 domain-containing protein tyrosine phosphatase 1/2; STLC, *S*-trityl-L-cysteine. **b**, EGFR is upregulated in hypoxia score-high ESCA and negatively correlates with six drugs (green lines, drug-sensitive). The hypomethylation of EGFR positively correlates with four of six drugs (magenta lines, drug-resistant). Downregulation of miR-375, miR-153-5p, miR-200a-3p and miR-146a-5p may upregulate EGFR, and positively correlates to four of the six drugs (magenta line, drug-resistant); $n = 21$ for hypoxia score-high ESCA samples, $n = 80$ for hypoxia score-low ESCA samples. Associations among hypoxia-associated mRNAs, DNA methylation, miRNAs and drug response were calculated by Spearman's rank correlation. The boxes in **b** show the median ± 1 quartile, with the whiskers extending from the hinge to the smallest or largest value within 1.5× IQR from the box boundaries.

downregulation of gene expression was consistent with the hypermethylation of promoter regions and the upregulation of miRNAs, and highly correlated with the response to anticancer drugs (Supplementary Fig. 7a). Furthermore, we observed significant correlations between protein expression and drug response, which is consistent with the correlations between mRNA expression and drug response (Supplementary Fig. 7b). Taken together, our results suggest that regulatory networks are affected in complicated ways

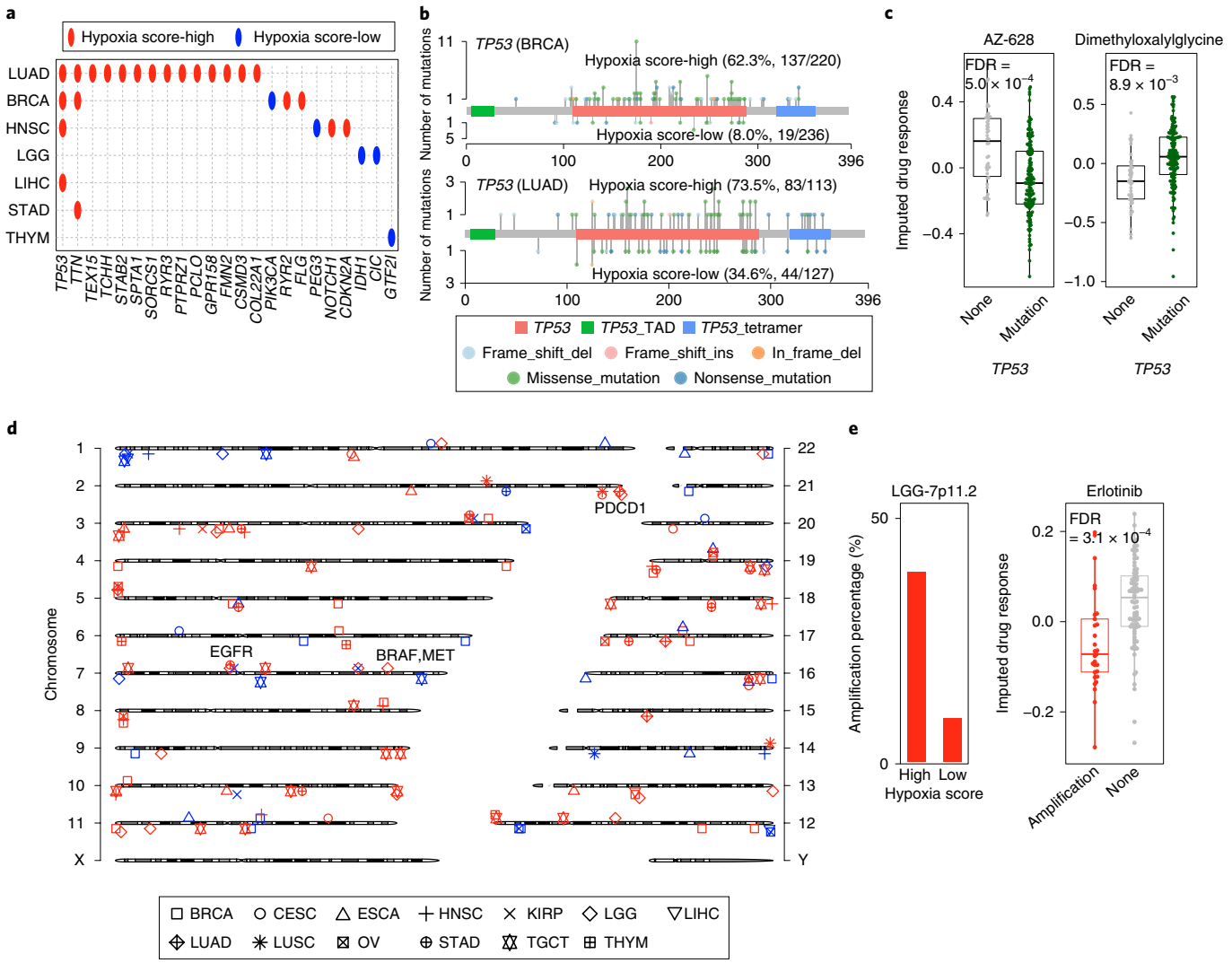

Fig. 6 | Hypoxia-associated somatic mutation and SCNA signatures. a, Hypoxia-associated somatic mutations across seven cancer types. The results show significantly higher mutation frequency in hypoxia score-high samples (red), and lower mutation frequency in hypoxia score-low samples (blue). **b**, *TP53* mutation signature in patients with hypoxia score-high (upper) and hypoxia score-low (bottom) tumours in BRCA and LUAD in the lollipop plots. The percentages of samples with the *TP53* mutation in hypoxia score-high and hypoxia score-low samples, respectively are summarized in parentheses. **c**, A two-sided Student's *t*-test was used to compare imputed drug response to AZ-628 and dimethyloxalylglycine in patients with HNSC with ($n=46$) or without ($n=138$) the *TP53* mutation. **d**, Chromosome plot displays the distributions of hypoxia-associated SCNAs with significant alterations in the tumour. Red indicates hypoxia score-high-associated SCNAs; blue indicates hypoxia score-low-associated SCNAs. The different shapes of the points indicate different cancer types. The position of the point above or below the chromosome, respectively, indicates the copy number gains or losses in different cancer types. **e**, A two-sided Student's *t*-test was used to compare the percentage of 7p11.2 amplification in hypoxia score-high and score-low LGG samples (left). Imputed drug response to erlotinib in patients with LGG with ($n=29$) or without ($n=79$) 7p11.2 amplification (right). Note that lower imputed drug responses on the *y* axis in panels **c** and **e** imply greater drug sensitivity. The boxes in **c** and **e** indicate the median ± 1 quartile, with the whiskers extending from the hinge to the smallest or largest value within 1.5× IQR from the box boundaries.

by the hypoxia microenvironment at multiple layers; these regulatory networks may largely affect drug response.

Hypoxia-associated somatic mutations and copy number alterations. To reveal the global pattern of hypoxia-associated mutations, we examined mutation frequency across multiple cancer types and identified hypoxia-associated mutated genes ranging from 1 in THYM to 14 in LUAD (Fig. 6a and Supplementary Fig. 8a). For example, tumour protein p53 (*TP53*) had significantly higher mutation frequency in hypoxia score-high tumours across multiple cancer types; 62.3% (137 out of 220) and 73.5% (83 out of 113) of samples had *TP53* mutations in hypoxia score-high BRCA and LUAD, while only 8.0% (19 out of 236) and 34.6% (44 out of 127) of samples had *TP53* mutations in hypoxia score-low BRCA and LUAD, respectively (Fig. 6b). This is consistent with previous reports that mutations of p53 contribute to diminished oxygen consumption[51]. We further observed that *TP53* mutations were associated with reduced drug response to the BRAF inhibitor, AZ-628 (FDR = 5.0×10^{-4}; Fig. 6c), and increased response to the hypoxia-inducible factor prolyl hydroxylase inhibitor dimethyloxalylglycine (FDR = 8.9×10^{-3}; Fig. 6c). In contrast, isocitrate dehydrogenase (NADP$^+$) 1, cytosolic (IDH1) has 95.5% (63 out of 66) mutation frequency in hypoxia score-low samples, whereas it only has 38.1% (32 out of 84) in hypoxia score-high samples in LGG. Mutation of

IDH1 promotes the degradation of HIF-1α[52], thus reducing the hypoxic effects in tumours and leading to better patient survival times (log-rank test, $P = 2.6 \times 10^{-13}$; Supplementary Fig. 8b).

Hypoxia can induce transient site-specific copy number gains in tumour cells[8]. We comprehensively analysed hypoxia-associated SCNAs across different cancer types and identified significantly hypoxia-associated SCNAs in 13 cancer types, ranging from 2 in THYM to 29 in BRCA (Figs. 3 and 6d; Supplementary Data 1). Notably, these hypoxia-associated SCNAs harbour several clinically actionable genes (Fig. 6d). In LGG, the 7q32.3 amplicon, which harbours *BRAF* and *MET* and leads to gefitinib resistance[53], occurred more frequently in hypoxia score-high samples (FDR = 0.045; Fig. 6d). The 7p11.2 amplicon, which harbours *EGFR*, occurred more frequently in hypoxia score-high LGG samples ($FDR = 6.5 \times 10^{-5}$; Fig. 6e). In particular, we observed that 7p11.2-amplified LGG tumours were more sensitive to erlotinib (two-sided Student's *t*-test, $FDR = 3.1 \times 10^{-4}$), an anti-EGFR drug (Fig. 6e), which is consistent with a previous study[54]. Deletion of 2q37.3 ($FDR = 4.2 \times 10^{-3}$) occurred more frequently in hypoxia score-high samples. This region harbours programmed cell death protein 1 (PDCD1), which is the target of pembrolizumab and nivolumab for cancer immunotherapy[55]. In addition, several other SCNAs occur more frequently in hypoxia score-low samples. For example, 7q31.2 amplification, which harbours *MET*, occurred more frequently in hypoxia score-low KIRP ($FDR = 5.3 \times 10^{-3}$). Deletion of 9p23, which harbours cyclin-dependent kinase inhibitor 2A and cyclin-dependent kinase 4 inhibitor B, occurred more frequently in hypoxia score-low BRCA (FDR = 0.014). These results suggest that the hypoxia microenvironment could affect tumour response to drugs, including immunotherapy drugs, by altering the somatic copy numbers.

Hypoxia-associated molecular signatures in clinically actionable genes and their therapeutic liability. To characterize the clinically applicable therapeutic implications of hypoxia-associated molecular signatures, we examined the molecular alterations between hypoxia score-high and score-low samples across five molecular dimensions of 121 clinically actionable genes targeted by 89 Food and Drug Administration (FDA)-approved drugs[56] (Fig. 7a and Supplementary Fig. 9a). We identified hypoxia-associated features, ranging from 6 features in sarcoma (SARC) to 93 in TGCT (Supplementary Fig. 9b). For example, EGFR was biased in hypoxia score-high samples with overexpression of total proteins or phosphorylated proteins in 8 cancer types (for example, ESCA, difference = 0.54, $FDR = 5.5 \times 10^{-5}$; bladder carcinoma (BLCA), difference = 0.42, $FDR = 7.1 \times 10^{-3}$), amplification in two cancer types (STAD, FDR = 0.022; LGG, $FDR = 6.5 \times 10^{-5}$) and hypomethylation in two cancer types (cervical squamous cell carcinoma and endocervical adenocarcinoma (CESC), difference = −0.29, $FDR = 1.8 \times 10^{-8}$; ESCA, difference = −0.24, $FDR = 4.5 \times 10^{-8}$). Strikingly, 90.9% (110 out of 121) of clinically actionable genes were associated with at least 1 type of hypoxia-associated molecular signature in at least 1 cancer type (Fig. 7a). Interestingly, several immunotherapeutic targets were also affected by hypoxia. PDCD1 (PD-1) was highly expressed in hypoxia score-low samples in LUSC, suggesting that PDCD1 inhibitors, such as nivolumab and pembrolizumab[57,58], could have better efficacy in hypoxia score-low tumours. We observed many more such incidences in hypoxia score-low samples (453) than in hypoxia score-high samples (237), which may partially explain why drugs are generally more effective in hypoxia score-low tumours. Patients with tumours having greater incidence of hypoxia score-high groups may benefit from combination treatment with hypoxia-targeted therapy.

We further evaluated the hypoxia effects on drug response in patient samples from imputed drug data[59] (Supplementary Data 3). Our comprehensive analysis of the hypoxia effects on clinically actionable genes could be linked to hypoxia effects on drug response directly[60] (Fig. 7a). For 21 FDA-approved anticancer drugs available in the GDSC database, we showed alterations of drug responses across multiple cancer types. Furthermore, we observed that the response to paclitaxel positively correlated (drug-resistant) with hypoxia status in CESC ($r_s = 0.40$, $FDR = 6.2 \times 10^{-4}$; Supplementary Fig. 10a,b), which is consistent with the resistance reported in a cervical cancer cell line[61]. We also observed that the response to Akt inhibitor VIII negatively correlated (drug-sensitive) with hypoxia status in LUAD ($r_s = -0.25$, FDR = 0.02; Supplementary Fig. 10a,b), which is consistent with the sensitivity reported for Akt inhibitor VIII in lung cancer cell lines[62]. These observations suggest that our analysis is reliable and provides meaningful clinical insights. Tumours under hypoxic conditions are resistant to many drugs, including erlotinib in LIHC ($r_s = 0.42$, $FDR = 1.5 \times 10^{-4}$) and lapatinib in KIRP ($r_s = 0.49$, $FDR = 7.1 \times 10^{-6}$), suggesting a potential clinical benefit of combining the cancer treatment with hypoxia-targeted therapy for patients with LIHC or KIRP. Strikingly, some tumours may become sensitive to several drugs under hypoxic conditions, such as thapsigargin in PAAD ($r_s = -0.66$, $FDR < 1.0 \times 10^{-55}$) and imatinib in HNSC ($r_s = -0.31$, $FDR = 4.3 \times 10^{-4}$), which suggests that patients with these cancers may not benefit from hypoxia-targeted therapy.

To directly validate our findings on drug response, we performed drug sensitivity experiments on selected drugs under a hypoxic condition (1% O_2) and a normoxic condition (21% O_2) in two lung cancer cell lines (A549 and H1299). Consistent with our computational prediction, our experimental results using the drugs camptothecin and bexarotene showed greater drug resistance under the hypoxic condition, whereas using the drugs Akt inhibitor VIII and PHA-665752 showed greater sensitivity under the hypoxic condition for both A549 and H1299 cell lines (Fig. 7b and Supplementary Fig. 10c). Furthermore, we observed that patients with advanced NSCLC with high hypoxia scores were associated with worse prognosis after sorafenib treatment (log-rank test, $P = 8.6 \times 10^{-3}$; Supplementary Fig. 10d) in a clinical trial[63,64] (trial no. NCT00411671, BATTLE Program: Sorafenib in Patients with NSCLC). Taken together, these results show that the hypoxia microenvironment largely affects tumour response to anticancer drugs; thus, the tumour hypoxia microenvironment should be considered to improve the efficacy of cancer therapy.

Discussion

Hypoxia induces a series of biological changes that contribute to tumourigenesis and are associated with resistance to chemotherapy, radiation therapy, drug therapy and immunotherapy. Therefore, understanding the effect of hypoxia on molecular signatures is crucial to improving the outcomes of cancer therapy. The degree of tumour hypoxia varies across cancer types. In this study, we first demonstrated the robustness of a 15-gene signature to define hypoxia status across multiple cancer types. Considering that the hypoxia gene signature is a relative signature, we then classified tumour samples into hypoxia score-high, score-low and score-intermediate groups based on this signature in each cancer type. Focusing on the comparison between hypoxia score-high and score-low groups in each cancer type, we adopted a well-controlled statistical approach—the propensity score algorithm—to control potential confounders, including sex, ethnicity, age at diagnosis, smoking status, tumour stage, histological type and tumour purity. In this way, we identified hypoxia-biased molecular signatures that are largely independent from the potential confounders across 21 cancer types. Our study provides a comprehensive view of hypoxia-associated molecular signatures, including mRNA, miRNA and protein expression, DNA methylation, somatic mutations and SCNAs. These molecular alterations that are driven by the hypoxia microenvironment will probably impact a broad range of biological processes, including metabolic reprogramming, angiogenesis, apoptosis and multiple signalling pathways. Our integrative

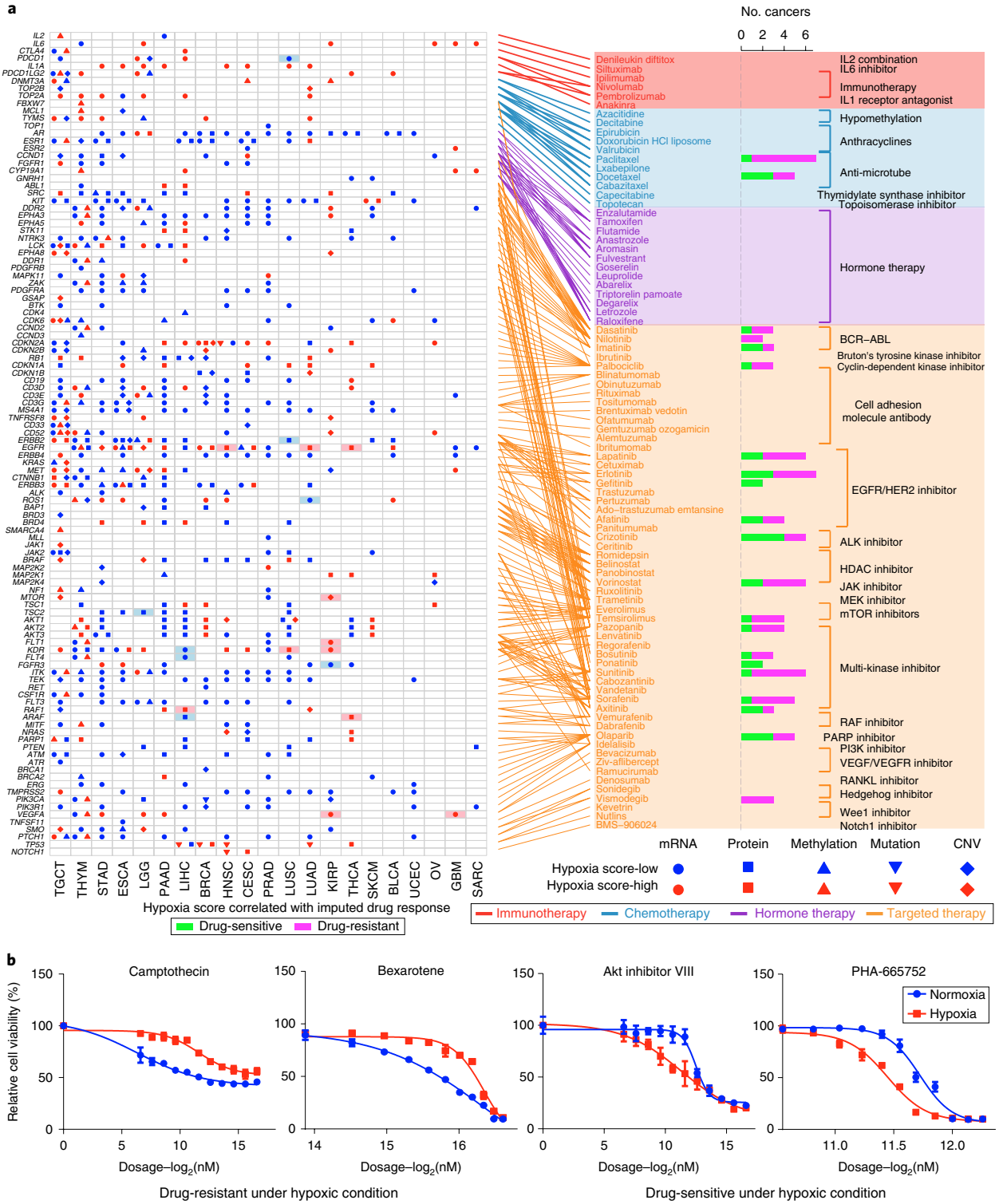

Fig. 7 | Hypoxia-associated molecular signatures in clinically actionable genes and effects on the response to individual drugs. a, Association between FDA-approved drugs and their linked clinically actionable genes (right) and alterations of these genes at mRNA, protein, DNA methylation, mutation and SCNA levels based on hypoxia score-high (red) or score-low (blue) samples across 21 cancer types (left). The different symbol shapes represent different types of molecular signatures. The filled cells indicate that the gene is a therapeutic target of clinical practice in the corresponding cancer type. The bar plots in the right panel indicate the number of cancer types with positive (drug-sensitive, magenta) and negative (drug-resistant, green) correlation between hypoxia score and drug response (Spearman's rank correlation). ALK, anaplastic lymphoma kinase; CNV, copy number variation; HDAC, histone deacetylase; HER2, human epidermal growth factor receptor; JAK, Janus kinase; MEK, mitogen-activated protein kinase; RANKL, receptor activator of nuclear factor κ-B ligand; VEGF, vascular endothelial growth factor; VEGFR, vascular endothelial growth factor receptor. **b**, Dose–response curves for the mean value of cell viability of camptothecin, bexarotene, Akt inhibitor-VIII and PHA-665752 in hypoxic (red, $n=4$) and normoxic (blue, $n=4$) conditions in the lung cancer cell line A549. Cell viability was normalized to that treated with dimethylsulfoxide. The error bars indicate the mean ± s.d. The sigmoidal dose–response curves were fitted to the data.

analysis further suggests that the hypoxia microenvironment can impact tumour molecular signatures at multi-omic levels through gene regulatory networks.

One striking observation is that 110 out of 121 (90.9%) clinically actionable genes are biased in at least one layer of molecular signatures across multiple cancer types. These clinically actionable genes are targets of FDA-approved cancer drugs, including drugs for immunotherapy, chemotherapy, hormone therapy and targeted therapy. Our comprehensive analysis demonstrates that many clinically actionable genes are biased towards hypoxia score-high samples and confirms that hypoxia-targeted therapy is an attractive cancer therapy, probably as a component of combination therapy targeting clinically actionable genes. Unfortunately, the results from several trials of hypoxia-targeted therapy have been disappointing[17,27–29]. This is probably because of our limited understanding of how molecular signatures are affected by the hypoxia microenvironment and our lack of rational combination therapies. Most clinical trials focus on overcoming the drug-resistant effects of hypoxia, while hypoxia may also result in increasing drug sensitivity in some patients[15]. These patients may not receive clinical benefit from hypoxia-targeted therapy and/or combination treatments. Thus, our systematic classification of hypoxia status and the identification of hypoxia-biased signatures have crucial clinical implications; this analysis can help to evaluate the clinical benefit of hypoxia-targeted therapy.

Our study has several limitations. First, large-scale tumour samples with multiple omic datasets (for example, TCGA) generally do not provide direct values for hypoxia status, for example, O_2 levels. Therefore, we had to indirectly infer the relative hypoxia status through the hypoxia gene signature in each cancer type, as described in previous studies[6,7,32]. We validated the performance of this hypoxia gene signature using independent datasets where hypoxia status is known. Second, large-scale datasets often provide the bulk of information across different cell types within a sample. With advancements in single-cell profiling technology, future efforts should take tumour heterogeneity into consideration. Third, our analyses provide a comprehensive catalogue of molecular alterations associated with hypoxia. Despite the causal effects demonstrated by many previous studies and a few cases within our experiments, further efforts are necessary to identify which alterations are directly affected by hypoxia. Finally, most clinical trials do not have the information of the hypoxia status of patients' tumours. Thus, we have limited data to further validate our observations in more rigorous clinical settings. Nonetheless, our study calls attention to the need to include tumour hypoxia status in future clinical studies.

Methods

Multi-omic data and clinical data for TCGA samples. Molecular data, including mRNA expression, miRNA expression, protein expression, DNA methylation, somatic mutations, SCNAs and clinical data, including tumour stage, histology subtype, sex and overall survival times, across 33 cancer types were downloaded from the TCGA data portal (https://portal.gdc.cancer.gov/). One gene may have multiple methylation probes; we selected the probe that most negatively correlated with the expression of the corresponding gene[39]. We downloaded tumour purity data from the Tumor IMmune Estimation Resource[65] (http://cistrome.org/TIMER/download.html). If not available, we obtained TCGA tumour purity data from a previous study[66] (https://doi.org/10.5281/zenodo.253193) to complement our data. Normalized metabolite levels of the 23 TCGA breast cancer samples were downloaded from a previous study[43]. We identified different metabolites using a two-sided Student's *t*-test ($P < 0.05$).

Classification of hypoxia status across different cancer types. We selected a 15-gene expression signature (*ACOT7*, *ADM*, *ALDOA*, *CDKN3*, *ENO1*, *LDHA*, *MIF*, *MRPS17*, *NDRG1*, *P4HA1*, *PGAM1*, *SLC2A1*, *TPI1*, *TUBB6* and *VEGFA*)[6] that has been shown to perform the best when classifying hypoxia status. This gene signature was defined based on gene function and analysis of in vivo co-expression patterns and was highly enriched for hypoxia-regulated pathways[6]. The hypoxia score for each tumour sample or cancer cell line was calculated by using gene set variation analysis[67] based on 15 mRNA-based hypoxia signatures. The Student's *t*-test was used to assess the statistical difference between hypoxic and normoxic conditions in different cancer cell lines. Spearman's rank correlation was used to assess the correlation among hypoxia scores based on different gene signatures. We kept 24 cancer types with a sample size ≥ 100, and filtered KIRC and COAD samples with relatively high mutation frequency in *VHL* (≥5%) to avoid the effects of pseudohypoxia in the tumours. To classify hypoxia status, we employed unsupervised hierarchical clustering[7] to cluster samples in each cancer type based on the 15 mRNA-based hypoxia signatures. The top three sub-clusters were assigned as hypoxia score-high, score-intermediate and score-low groups in each cancer type. We included 21 cancer types with ≥ 30 samples in both hypoxia score-high and hypoxia score-low groups for further analysis (Supplementary Fig. 2 and Supplementary Table 2). To avoid the confounding factors from the potential mixture, we excluded samples from the hypoxia score-intermediate group from further analysis.

Identification of alterations between hypoxia score-high and hypoxia score-low tumours. To balance the potentially confounding factors (such as tumour stage, histology subtype and the other factors listed previously) between hypoxia score-high and hypoxia score-low groups, we performed the propensity score algorithm[39,40]. Briefly, we first calculated the propensity score using logistic regression with hypoxia status as a variable, and performed matching weights[38] to reweight samples based on their propensity scores. We considered the clinical confounding factors to be balanced between weighted hypoxia score-high and score-low samples if the standardized difference between their weighted propensity scores was < 10%. We then compared the molecular data between these two balanced groups and calculated the *P* values and FDRs. To eliminate random noise in signal detection, we used permutation tests by randomly selecting the hypoxia score-high or score-low labels of patient samples and repeated these steps 100 times. We calculated the ratio of the appearance of a significant feature set in these permuted datasets and retained the feature sets with a permutation test of $P < 0.05$ for further analysis. The statistical significance for each molecular data type in each cancer type is as follows: mRNA and miRNA expression: fold change > 2, FDR < 0.05; total protein or phosphorylated protein: difference > 0.2, FDR < 0.05; DNA methylation: difference > 0.2, FDR < 0.05; somatic mutation and SCNA: FDR < 0.05.

Analysis of clinically actionable genes and drug response. We downloaded clinically actionable genes identified as targets of FDA-approved therapeutic drugs or biomarkers from a previous study[56] (https://software.broadinstitute.org/cancer/cga/target). We collected the therapeutic drugs and their prescription information from the FDA Drug Approvals and Databases site (https://www.fda.gov/Drugs/InformationOnDrugs/)[60]. We retained clinically actionable genes with the corresponding drugs as therapeutic targets for further analysis. To assess drug response in cancer cell lines, we downloaded the drug sensitivity area under the dose–response curve (AUC) and gene expression profiles for cancer cell lines from the GDSC (http://www.cancerrxgene.org/downloads)[44]. We calculated the Spearman's rank correlation between gene expression and the AUCs from the GDSC[68] and used Spearman's rank correlation coefficient $|r_s| > 0.3$ and FDR < 0.05 for statistical significance.

To assess the drug response in TCGA patient samples, we downloaded the imputed tumour response to 138 anticancer drugs in cancer patients from a previous study[59]. We calculated the correlation between imputed drug response and hypoxia-associated mRNA expression, miRNA expression, protein expression and DNA methylation using Spearman's rank correlation, considering $|r_s| > 0.2$ and FDR < 0.05 for statistical significance. To compare the imputed drug response between groups with or without mutations and SCNAs, we used the Student's *t*-test and considered FDR < 0.05 as statistically significant.

Cell culture and reagents. A549 and H1299 were purchased from the American Type Culture Collection and Characterized Cell Line Core Facility (MD Anderson Cancer Center) and were cultured in DMEM supplemented with 10% fetal bovine serum (Gibco) at 37 °C in 5% CO_2 (v/v). Akt inhibitor VIII was purchased from Cayman Chemical (catalogue no. 612847-09-3); PHA-665752 (catalogue no. S1070), camptothecin (catalogue no. S1288) and bexarotene (catalogue no. S2098) were purchased from Selleck Chemicals.

Cell proliferation assay. The effect of the drug on cell proliferation was determined using a CellTiter 96 AQueous One Solution Cell Proliferation Assay Kit (Promega) according to the manufacturer's instructions. Cells were plated in 96-well plates (4 replicates per condition). The following day, cells were treated with a range of drug concentrations prepared by serial dilution. Plates were incubated under normoxic conditions (37 °C, 5% CO_2, 21% O_2) or under hypoxic conditions (37 °C, 5% CO_2, 1% O_2). After 3 d of treatment, assays were performed by adding 20 µl of the CellTiter 96 AQueous One Solution Reagent directly to the culture wells, incubating for 1 h and then recording absorbance at 490 nm with an EnVision Plate Reader (PerkinElmer). Relative growth was normalized to the untreated samples in each group. Drug response data analysis was performed with Prism version 7.00 (GraphPad software).

Analysis of clinical trial data. We examined clinical trials with data of related drugs and cancer types in our study from ClinicalTrials.gov (https://clinicaltrials.gov/). We identified only one clinical trial (NCT00411671, BATTLE Program:

Sorafenib in Patients With NSCLC) that had both detailed clinical outcomes and mRNA expression data (NCBI GEO accession no. GSE33072). Patients who received sorafenib treatment were classified into two groups based on the hypoxia scores of their tumour samples. We used a log-rank test to assess the difference in the overall survival times between the two groups.

Reporting Summary. Further information on research design is available in the Nature Research Reporting Summary linked to this article.

Code availability

Codes were implemented in R and have been deposited in GitHub: https://github.com/youqiongye/HAMFA.

Data availability

All data supporting the findings of the current study are listed in Supplementary Tables 1–3 and Supplementary Data 1–3.

Received: 15 June 2018; Accepted: 14 February 2019;
Published online: 18 March 2019

References

1. Bertout, J. A., Patel, S. A. & Simon, M. C. The impact of O_2 availability on human cancer. *Nat. Rev. Cancer* **8**, 967–975 (2008).
2. Walsh, J. C. et al. The clinical importance of assessing tumor hypoxia: relationship of tumor hypoxia to prognosis and therapeutic opportunities. *Antioxid. Redox Signal.* **21**, 1516–1554 (2014).
3. Wigerup, C., Påhlman, S. & Bexell, D. Therapeutic targeting of hypoxia and hypoxia-inducible factors in cancer. *Pharmacol. Ther.* **164**, 152–169 (2016).
4. Harris, B. H. L., Barberis, A., West, C. M. L. & Buffa, F. M. Gene expression signatures as biomarkers of tumour hypoxia. *Clin. Oncol. (R. Coll. Radiol.)* **27**, 547–560 (2015).
5. Fox, N. S., Starmans, M. H. W., Haider, S., Lambin, P. & Boutros, P. C. Ensemble analyses improve signatures of tumour hypoxia and reveal inter-platform differences. *BMC Bioinformatics* **15**, 170 (2014).
6. Buffa, F. M., Harris, A. L., West, C. M. & Miller, C. J. Large meta-analysis of multiple cancers reveals a common, compact and highly prognostic hypoxia metagene. *Br. J. Cancer* **102**, 428–435 (2010).
7. Thienpont, B. et al. Tumour hypoxia causes DNA hypermethylation by reducing TET activity. *Nature* **537**, 63–68 (2016).
8. Black, J. C. et al. Hypoxia drives transient site-specific copy gain and drug-resistant gene expression. *Genes Dev.* **29**, 1018–1031 (2015).
9. Amelio, I. & Melino, G. The p53 family and the hypoxia-inducible factors (HIFs): determinants of cancer progression. *Trends Biochem. Sci.* **40**, 425–434 (2015).
10. Marhold, M. et al. HIF1α regulates mTOR signaling and viability of prostate cancer stem cells. *Mol. Cancer Res.* **13**, 556–564 (2015).
11. Krock, B. L., Skuli, N. & Simon, M. C. Hypoxia-induced angiogenesis: good and evil. *Genes Cancer* **2**, 1117–1133 (2011).
12. Masoud, G. N. & Li, W. HIF-1α pathway: role, regulation and intervention for cancer therapy. *Acta Pharm. Sin. B* **5**, 378–389 (2015).
13. Dang, K. & Myers, K. A. The role of hypoxia-induced miR-210 in cancer progression. *Int. J. Mol. Sci.* **16**, 6353–6372 (2015).
14. Koumenis, C. et al. Regulation of protein synthesis by hypoxia via activation of the endoplasmic reticulum kinase PERK and phosphorylation of the translation initiation factor eIF2α. *Mol. Cell. Biol.* **22**, 7405–7416 (2002).
15. Wilson, W. R. & Hay, M. P. Targeting hypoxia in cancer therapy. *Nat. Rev. Cancer* **11**, 393–410 (2011).
16. Lara, P. C. et al. Severe hypoxia induces chemo-resistance in clinical cervical tumors through MVP over-expression. *Radiat. Oncol.* **4**, 29 (2009).
17. Samanta, D., Gilkes, D. M., Chaturvedi, P., Xiang, L. & Semenza, G. L. Hypoxia-inducible factors are required for chemotherapy resistance of breast cancer stem cells. *Proc. Natl Acad. Sci. USA* **111**, E5429–E5438 (2014).
18. Gatenby, R. A. et al. Oxygen distribution in squamous cell carcinoma metastases and its relationship to outcome of radiation therapy. *Int. J. Radiat. Oncol. Biol. Phys.* **14**, 831–838 (1988).
19. Minakata, K. et al. Hypoxia induces gefitinib resistance in non-small-cell lung cancer with both mutant and wild-type epidermal growth factor receptors. *Cancer Sci.* **103**, 1946–1954 (2012).
20. Scharping, N. E., Menk, A. V., Whetstone, R. D., Zeng, X. & Delgoffe, G. M. Efficacy of PD-1 blockade is potentiated by metformin-induced reduction of tumor hypoxia. *Cancer Immunol. Res.* **5**, 9–16 (2017).
21. Reddy, K. R., Guan, Y., Qin, G., Zhou, Z. & Jing, N. Combined treatment targeting HIF-1α and Stat3 is a potent strategy for prostate cancer therapy. *Prostate* **71**, 1796–1809 (2011).
22. Seeber, L. M. S., Zweemer, R. P., Verheijen, R. H. M. & van Diest, P. J. Hypoxia-inducible factor-1 as a therapeutic target in endometrial cancer management. *Obstet. Gynecol. Int.* **2010**, 580971 (2010).
23. Liu, S. K. et al. A novel poly(ADP-ribose) polymerase inhibitor, ABT-888, radiosensitizes malignant human cell lines under hypoxia. *Radiother. Oncol.* **88**, 258–268 (2008).
24. Jiang, Y. et al. Hypoxia potentiates the radiation-sensitizing effect of olaparib in human non-small cell lung cancer xenografts by contextual synthetic lethality. *Int. J. Radiat. Oncol. Biol. Phys.* **95**, 772–781 (2016).
25. Patel, P. H. et al. Hypoxia-inducible factor (HIF) 1α and 2α levels in cell lines and human tumor predicts response to sunitinib in renal cell carcinoma (RCC). *J. Clin. Oncol.* **26**, 5008 (2008).
26. Salem, A. et al. Targeting hypoxia to improve non-small cell lung cancer outcome. *J. Natl Cancer Inst.* **110**, 14–30 (2018).
27. Ramanathan, R. K. et al. A randomized phase II study of PX-12, an inhibitor of thioredoxin in patients with advanced cancer of the pancreas following progression after a gemcitabine-containing combination. *Cancer Chemother. Pharmacol.* **67**, 503–509 (2011).
28. Williamson, S. K. et al. Phase III trial of paclitaxel plus carboplatin with or without tirapazamine in advanced non-small-cell lung cancer: Southwest Oncology Group Trial S0003. *J. Clin. Oncol.* **23**, 9097–9104 (2005).
29. Davidson, A. et al. A phase III randomized trial of adding topical nitroglycerin to first-line chemotherapy for advanced nonsmall-cell lung cancer: the Australasian lung cancer trials group NITRO trial. *Ann. Oncol.* **26**, 2280–2286 (2015).
30. Chang, K. et al. The Cancer Genome Atlas Pan-Cancer analysis project. *Nat. Genet.* **45**, 1113–1120 (2013).
31. Xiang, Y., Ye, Y., Zhang, Z. & Han, L. Maximizing the utility of cancer transcriptomic data. *Trends Cancer* **4**, 823–837 (2018).
32. Haider, S. et al. Genomic alterations underlie a pan-cancer metabolic shift associated with tumour hypoxia. *Genome Biol.* **17**, 140 (2016).
33. Winter, S. C. et al. Relation of a hypoxia metagene derived from head and neck cancer to prognosis of multiple cancers. *Cancer Res.* **67**, 3441–3449 (2007).
34. Hu, Z. et al. A compact VEGF signature associated with distant metastases and poor outcomes. *BMC Med.* **7**, 9 (2009).
35. Bratslavsky, G., Sudarshan, S., Neckers, L. & Linehan, W. M. Pseudohypoxic pathways in renal cell carcinoma. *Clin. Cancer Res.* **13**, 4667–4671 (2007).
36. Mertins, P. et al. Proteogenomics connects somatic mutations to signalling in breast cancer. *Nature* **534**, 55–62 (2016).
37. Zhang, H. et al. Integrated proteogenomic characterization of human high-grade serous ovarian cancer. *Cell* **166**, 755–765 (2016).
38. Li, L. & Greene, T. A weighting analogue to pair matching in propensity score analysis. *Int. J. Biostat.* **9**, 215–234 (2013).
39. Yuan, Y. et al. Comprehensive characterization of molecular differences in cancer between male and female patients. *Cancer Cell* **29**, 711–722 (2016).
40. Deng, J. et al. Comparative genomic analysis of esophageal squamous cell carcinoma between Asian and Caucasian patient populations. *Nat. Commun.* **8**, 1533 (2017).
41. Mermel, C. H. et al. GISTIC2.0 facilitates sensitive and confident localization of the targets of focal somatic copy-number alteration in human cancers. *Genome Biol.* **12**, R41 (2011).
42. Eales, K. L., Hollinshead, K. E. R. & Tennant, D. A. Hypoxia and metabolic adaptation of cancer cells. *Oncogenesis* **5**, e190 (2016).
43. Tang, X. et al. A joint analysis of metabolomics and genetics of breast cancer. *Breast Cancer Res* **16**, 415 (2014).
44. Yang, W. et al. Genomics of Drug Sensitivity in Cancer (GDSC): a resource for therapeutic biomarker discovery in cancer cells. *Nucleic Acids Res.* **41**, D955–D961 (2013).
45. Glück, A. A., Aebersold, D. M., Zimmer, Y. & Medová, M. Interplay between receptor tyrosine kinases and hypoxia signaling in cancer. *Int. J. Biochem. Cell Biol.* **62**, 101–114 (2015).
46. Jones, P. A. Functions of DNA methylation: islands, start sites, gene bodies and beyond. *Nat. Rev. Genet.* **13**, 484–492 (2012).
47. Qu, Y. et al. MiR-139-5p inhibits HGTD-P and regulates neuronal apoptosis induced by hypoxia-ischemia in neonatal rats. *Neurobiol. Dis.* **63**, 184–193 (2014).
48. Tanizaki, J. et al. MET tyrosine kinase inhibitor crizotinib (PF-02341066) shows differential antitumor effects in non-small cell lung cancer according to MET alterations. *J. Thorac. Oncol.* **6**, 1624–1631 (2011).
49. Li, C. et al. Fibronectin induces epithelial-mesenchymal transition in human breast cancer MCF-7 cells via activation of calpain. *Oncol. Lett.* **13**, 3889–3895 (2017).
50. Georgescu, M. M. PTEN tumor suppressor network in PI3K-Akt pathway control. *Genes Cancer* **1**, 1170–1177 (2010).
51. Kawauchi, K., Araki, K., Tobiume, K. & Tanaka, N. p53 regulates glucose metabolism through an IKK-NF-κB pathway and inhibits cell transformation. *Nat. Cell Biol.* **10**, 611–618 (2008).
52. Chesnelong, C. et al. Lactate dehydrogenase A silencing in IDH mutant gliomas. *Neuro-oncology* **16**, 686–695 (2014).
53. Engelman, J. A. et al. MET amplification leads to gefitinib resistance in lung cancer by activating ERBB3 signaling. *Science* **316**, 1039–1043 (2007).

54. Schulte, A. et al. Erlotinib resistance in EGFR-amplified glioblastoma cells is associated with upregulation of EGFRvIII and PI3Kp110δ. *Neuro-oncology* **15**, 1289–1301 (2013).
55. Topalian, S. L., Taube, J. M., Anders, R. A. & Pardoll, D. M. Mechanism-driven biomarkers to guide immune checkpoint blockade in cancer therapy. *Nat. Rev. Cancer* **16**, 275–287 (2016).
56. Van Allen, E. M. et al. Whole-exome sequencing and clinical interpretation of formalin-fixed, paraffin-embedded tumor samples to guide precision cancer medicine. *Nat. Med.* **20**, 682–688 (2014).
57. Reck, M. et al. Pembrolizumab versus chemotherapy for PD-L1-positive non-small-cell lung cancer. *N. Engl. J. Med.* **375**, 1823–1833 (2016).
58. Kazandjian, D. et al. FDA approval summary: nivolumab for the treatment of metastatic non-small cell lung cancer with progression on or after platinum-based chemotherapy. *Oncologist* **21**, 634–642 (2016).
59. Geeleher, P. et al. Discovering novel pharmacogenomic biomarkers by imputing drug response in cancer patients from large genomics studies. *Genome Res.* **27**, 1743–1751 (2017).
60. Ye, Y. et al. The genomic landscape and pharmacogenomic interactions of clock genes in cancer chronotherapy. *Cell Syst.* **6**, 314–328.e2 (2018).
61. Shen, Y. et al. MiR-375 is upregulated in acquired paclitaxel resistance in cervical cancer. *Br. J. Cancer* **109**, 92–99 (2013).
62. Stegeman, H. et al. Interaction between hypoxia, AKT and HIF-1 signaling in HNSCC and NSCLC: implications for future treatment strategies. *Future Sci. OA* **2**, FSO84 (2016).
63. Byers, L. A. et al. An epithelial-mesenchymal transition gene signature predicts resistance to EGFR and PI3K inhibitors and identifies Axl as a therapeutic target for overcoming EGFR inhibitor resistance. *Clin. Cancer Res.* **19**, 279–290 (2013).
64. Kim, E. S. et al. The BATTLE trial: personalizing therapy for lung cancer. *Cancer Discov.* **1**, 44–53 (2011).
65. Li, B. et al. Comprehensive analyses of tumor immunity: implications for cancer immunotherapy. *Genome Biol.* **17**, 174 (2016).
66. Zheng, X., Zhang, N., Wu, H. J. & Wu, H. Estimating and accounting for tumor purity in the analysis of DNA methylation data from cancer studies. *Genome Biol.* **18**, 17 (2017).
67. Hänzelmann, S., Castelo, R. & Guinney, J. GSVA: gene set variation analysis for microarray and RNA-Seq data. *BMC Bioinformatics* **14**, 7 (2013).
68. Xiang, Y. et al. Comprehensive characterization of alternative polyadenylation in human cancer. *J. Natl Cancer Inst.* **110**, 379–389 (2018).

Acknowledgements

This work was supported by the Cancer Prevention & Research Institute of Texas (grant no. RR150085 to L.H., grant no. RP140462 to H.L., grant nos. RP150094 and RP180259 to C.L. and grant no. R1218 to L.Y.); the National Institutes of Health (grant nos. CA168394, CA098258 and CA143883 to G.B.M., grant no. CA175486 to H.L., grant no. CA209851 to H.L. and G.B.M., grant no. R00DK094981, 1R01CA218025 and 1R01CA231011 to C.L., grant no. R00CA166527 and 1R01CA218036 to L.Y. and grant no. R01 HL137990 and 1R01HL136969 to Y.X.). Department of Defense Breakthrough Awards were granted to C.L. and L.Y. (award no. BC180196 to C.L. and award no. BC151465 to L.Y.). The American Association for Cancer Research–Bayer Innovation and Discovery Grant (no. 18-80-44) and Andrew Sabin Family Foundation Fellows Award were awarded to L.Y., J.G. was awarded an MD Anderson Physician Scientist Award, a Khalifa Physician Scientist Award, an Andrew Sabin Family Foundation Fellows Award, an MD Anderson Faculty Scholar Award and a Doris Duke Charitable Foundation Career Development Award (award no. 2018097). The National Natural Science Foundation of China supported S.Z. with grant nos. 81822034 and 81773119. We gratefully acknowledge contributions from the TCGA Research Network. We thank L.-A. Chastain for editorial assistance.

Author contributions

L.H. conceived and supervised the project. Y.Ye and L.H. designed and performed the research. Y.Ye, H.C., Y.Yuan, Y.Xiang, H.R., Z.Z., A.S., H.Z., L.L. and L.D. performed the data analysis. Y.Ye, Q.H. K.L., C.L., L.Y. and L.H. performed the drug tests. Y.Ye, Y.L., B.Z., S.Z., J.G., E.J., S.H.L., L.W., Y.Xia, L.Y., C.L., G.B.M., H.L. and L.H. interpreted the results. Y.Ye, Q.H., G.B.M., H.L. and L.H. wrote the manuscript with input from all other authors.

Competing interests

G.B.M. has sponsored research support from AstraZeneca, Critical Outcomes Technologies, Karus Therapeutics, Illumina, Immunomet, NanoString, Tarveda Therapeutics and Immunomet. He is on the Scientific Advisory Boards of AstraZeneca, Critical Outcomes Technologies, Immunomet, Ionis Pharmaceuticals, Nuevolution, Symphogen and Tarveda Therapeutics. H.L. is a shareholder and scientific advisor of Precision Scientific and Eagle Nebula. J.G. serves as a consultant for ARMO Biosciences, AstraZeneca, Jounce Therapeutics, Nektar and Pfizer.

Additional information

Supplementary information is available for this paper at https://doi.org/10.1038/s42255-019-0045-8.

Reprints and permissions information is available at www.nature.com/reprints.

Correspondence and requests for materials should be addressed to L.Y., G.B.M., H.L. or L.H.

Publisher's note: Springer Nature remains neutral with regard to jurisdictional claims in published maps and institutional affiliations.

nature research

Corresponding author(s): Leng Han, Han Liang, Gordon B. Mills, Liuqing Yang

Last updated by author(s): 2/1/2019

Reporting Summary

Nature Research wishes to improve the reproducibility of the work that we publish. This form provides structure for consistency and transparency in reporting. For further information on Nature Research policies, see Authors & Referees and the Editorial Policy Checklist.

Statistics

For all statistical analyses, confirm that the following items are present in the figure legend, table legend, main text, or Methods section.

n/a	Confirmed	
☐	☒	The exact sample size (*n*) for each experimental group/condition, given as a discrete number and unit of measurement
☐	☒	A statement on whether measurements were taken from distinct samples or whether the same sample was measured repeatedly
☐	☒	The statistical test(s) used AND whether they are one- or two-sided *Only common tests should be described solely by name; describe more complex techniques in the Methods section.*
☐	☒	A description of all covariates tested
☐	☒	A description of any assumptions or corrections, such as tests of normality and adjustment for multiple comparisons
☐	☒	A full description of the statistical parameters including central tendency (e.g. means) or other basic estimates (e.g. regression coefficient) AND variation (e.g. standard deviation) or associated estimates of uncertainty (e.g. confidence intervals)
☒	☐	For null hypothesis testing, the test statistic (e.g. *F*, *t*, *r*) with confidence intervals, effect sizes, degrees of freedom and *P* value noted *Give P values as exact values whenever suitable.*
☒	☐	For Bayesian analysis, information on the choice of priors and Markov chain Monte Carlo settings
☐	☒	For hierarchical and complex designs, identification of the appropriate level for tests and full reporting of outcomes
☐	☒	Estimates of effect sizes (e.g. Cohen's *d*, Pearson's *r*), indicating how they were calculated

Our web collection on statistics for biologists contains articles on many of the points above.

Software and code

Policy information about availability of computer code

Data collection	No software was used for data collection.
Data analysis	All data analysis was performed by R programming and GraphPad Prism v 7.00. R codes are deposited in GitHub: https://github.com/youqiongye/HAMFA.

For manuscripts utilizing custom algorithms or software that are central to the research but not yet described in published literature, software must be made available to editors/reviewers. We strongly encourage code deposition in a community repository (e.g. GitHub). See the Nature Research guidelines for submitting code & software for further information.

Data

Policy information about availability of data

All manuscripts must include a data availability statement. This statement should provide the following information, where applicable:

- Accession codes, unique identifiers, or web links for publicly available datasets
- A list of figures that have associated raw data
- A description of any restrictions on data availability

All data supporting the findings of the current study are listed in the supplementary tables 1-3 and Supplementary data files 1-3.

Field-specific reporting

Please select the one below that is the best fit for your research. If you are not sure, read the appropriate sections before making your selection.

☒ Life sciences ☐ Behavioural & social sciences ☐ Ecological, evolutionary & environmental sciences

Life sciences study design

All studies must disclose on these points even when the disclosure is negative.

Sample size	In our pan-cancer analysis, we analyzed all tumors with multi-omics data and clinical data from TCGA data portal (https://tcga-data.nci.nih.gov/tcga/) (n = 9686). We included 21 cancer types with ≥ 30 samples in both hypoxia score-high and hypoxia score-low groups for further analysis as listed in Supplementary Table 2. Metabolic analysis was performed in 23 TCGA breast cancer samples with metabolite profiles. Drug responses for 1,074 cancer cell lines were obtained from Drug Sensitivity in Cancer (GDSC, http://www.cancerrxgene.org/downloads). For drug response experiments, we used 4 biological replicates in the paper.
Data exclusions	We kept 24 cancer types with sample size ≥ 100, and filtered KIRC and COAD samples with relatively high mutation frequency in VHL (≥ 5%) to avoid effects of pseudo-hypoxia in the tumors. We included 21 cancer types with ≥ 30 samples in both hypoxia score-high and hypoxia score-low groups for further analysis
Replication	All data analyses and experimental findings are reproducible.
Randomization	Samples were allocated to groups based on hypoxia status, mutations status, and DNA copy number status if applicable.
Blinding	All data was obtained from public data resources, so blinding was not relevant.

Reporting for specific materials, systems and methods

We require information from authors about some types of materials, experimental systems and methods used in many studies. Here, indicate whether each material, system or method listed is relevant to your study. If you are not sure if a list item applies to your research, read the appropriate section before selecting a response.

Materials & experimental systems

n/a	Involved in the study
☒	☐ Antibodies
☐	☒ Eukaryotic cell lines
☒	☐ Palaeontology
☒	☐ Animals and other organisms
☒	☐ Human research participants
☒	☐ Clinical data

Methods

n/a	Involved in the study
☒	☐ ChIP-seq
☒	☐ Flow cytometry
☒	☐ MRI-based neuroimaging

Eukaryotic cell lines

Policy information about cell lines

Cell line source(s)	A549 and H1299 cell lines were purchased from American Type Culture Collection (ATCC) and Characterized Cell Line Core Facility (MD Anderson Cancer Center), respectively.
Authentication	A549 cell line was authenticated by ATCC using Short tandem repeat (STR) profiling. H1299 cell line was authenticated by Characterized Cell Line Core Facility at MD Anderson Cancer Center using STR profiling.
Mycoplasma contamination	Tests of mycoplasma contamination in both cell lines were negative.
Commonly misidentified lines (See ICLAC register)	None of the cell lines used are listed in the ICLAC database.